[19] Pitas, I.
Digital Image Processing Algorithms (International Series in Acoustic, Speech, and Signal Processing).
Upper Saddle River, NJ: Prentice-Hall, 1993.

[20] Foresti, G. L., Frassinetti, M., Galati, G., Marti, F., Pellegrini, P., and Regazzoni, C. S.
Image processing applications to airport surface movements radar surveillance and tracking.
In *Proceedings of the 20th IEEE International Conference on Industrial Electronics, Control and Instrumentation*, Bologna, Italy, Sept. 5–9, 1994.

[21] Galati, G., Leonardi, M., and Magarò, P.
Bearing angle and shape extraction features in high resolution surface movement radar.
RTA NATO SET-059, Budapest, Hungary, Oct. 15–17, 2003.

[22] Galati, G., Leonardi, M., and Magarò, P.
Analysis and evaluation of different tracking algorithms based on roadmap information.
RTA NATO SET-059, Budapest, Hungary, Oct. 15–17, 2003.

[23] Bar Shalom, Y. and Blair, D.
Multitargets-Multisensors Tracking Applications.
Norwood, MA: Artech House, 2000.

[24] Bar Shalom, Y. and Li, X-R.
Estimation and Tracking: Principles, Techniques and Software.
Norwood, MA: Artech House, 1993.

[25] Bar Shalom, Y. and Li, X-R.
Multitarget-Multisensor Tracking: Principles and Techniques.
Storrs, CT: YBS Publishing, 1995.

[26] Brookner, E.
Tracking and Kalman Filtering Made Easy.
Hoboken, NJ: Wiley, 1998.

[27] Blackman, P.
Design and Analysis of Modern Tracking Systems.
Norwood, MA: Artech House, 1999.

[28] Kirubarajan, T., Bar-Shalom, Y., and Pattipati, K. R.
Topography-based VS-IMM estimator for large-scale ground target tracking.
In *Proceedings of the IEE Colloquium on Target Tracking*, London, Nov. 1999, 11/1–11/4.

[29] Kirubarajan, T., Bar-Shalom, Y., Pattipati, K. R., and Kadar, I.
Ground target tracking with variable structure IMM estimator.
IEEE Transactions on Aerospace and Electronic Systems, **36**, 1 (2000), 26–46.

[30] García Herrero, J., Besada Portas, J. A., and Casar Corredera, J. R.
Use of map information for tracking targets on airport surface.
IEEE Transactions on Aerospace and Electronic Systems, **39**, 2 (Apr. 2003), 675–694.

[31] García Herrero, J., Besada Portas, J. A., Jiménez Rodríguez, F. J., and Casar Corredera, J. R.
Surface movement radar data processing methods for airport surveillance.
IEEE Transactions on Aerospace and Electronic Systems, **37**, 2 (Apr. 2001), 563–586.

Zero-Knowledge Adaptive Beamforming using Analog Signal Processor for Satellite Tracking Applications with an Experimental Comparison to a Digital Implementation

A novel analog circuit for adaptive beamforming in an ultra low profile stair-planar phased array antenna system for mobile broadcast satellite reception in Ku-band is presented and its performance experimentally compared with digital beamforming control. The novelty of this method is that it performs gradient descent using an entirely analog feedback path. The beamforming algorithm compensates for the fabrication inaccuracies of the microwave components and variations in their characteristics due to ambient changes. Neither a priori knowledge of the satellite's direction nor the phase-voltage characteristic of the phase shifters are required in this implementation which results in eliminating an expensive laborious calibration procedure. The circuit performs continuous-time gradient descent using simultaneous perturbation gradient estimation. Field tests were performed in a realistic scenario using a satellite signal. The optimizer can converge in less than 50 ms and easily tracks antenna motions of greater than $60^\circ/\mathrm{s}$. There are significant savings in terms of system cost, power consumption, and system integration complexity by switching to an integrated analog implementation.

I. INTRODUCTION

Although dish antennas are suitable for most digital satellite TV applications, low profile antenna arrays are much more popular for mobile applications (land/sea/air transportation) because of aesthetics and low aerodynamic drag. In mobile applications extremely precise mechanical tracking is needed to compensate for the roll, pitch, and yaw motions in order to keep the antenna pointed at the satellite due to the high-gain narrowbeam antenna pattern. The mechanical tracking performance requirements can be

Manuscript received February 25, 2008; revised September 30, 2008 and April 1, 2009; released for publication June 15, 2009.

IEEE Log No. T-AES/46/3/937990.

Refereeing of this contribution was handled by M. Rice.

This work was supported by Research in Motion (RIM), the Natural Sciences and Engineering Research Council of Canada (NSERC), and Intelwaves Technolgies. The work was performed in collaboration with the iMARS team at the University of Waterloo.

This work was presented in part at the IEEE Antennas and Propagation Society International Symposium, 2008.

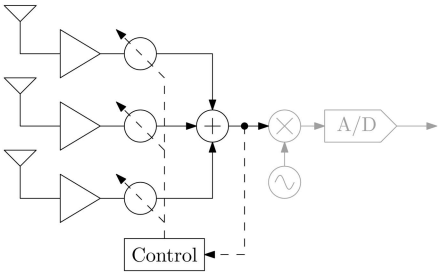

Fig. 1. Beamforming architecture.

significantly relaxed by utilizing adaptive electronic beamforming in order to continuously adapt the antenna pattern for maximum signal reception.

We have recently developed a 6 cm tall antenna array for Ku-band satellite TV reception on moving vehicles [2, 3]. A summary of mobile direct broadcast satellite (DBS) requirements and the performance achieved by our system is presented in Section II. In order to further reduce the cost of this system, we investigated the option of replacing the digital beamforming algorithm, including associated hardware and software, by an analog circuit which performs gradient descent beamforming. In contrast to most analog beamforming algorithms [4, 5] that digitally control the analog phase shifters, this method uses entirely analog control.

The beamforming architecture consists of microwave beamforming using analog phase shifters as the adjustment weights (Fig. 1).[1] Only three antenna elements are shown for illustration purposes, but each polarization has 17 subarrays. The system contains a set of subarrays, one for left-hand polarization and one for right-hand polarization, for a total of 34 subarrays for the whole antenna system. Each received signal is amplified by a low noise amplifier (LNA) then passed through an analog phase shifter.[2] All signals are then combined, and the resulting signal is converted using a custom-made low noise block (LNB) from the original RF frequency of 12.2–12.7 GHz to an IF frequency of 950–1450 MHz. The signal then is provided to an off-the-shelf digital satellite TV receiver which incorporates further down-conversion as well as digitization of the signal. This part of the diagram is grayed out because it is outside the scope of our work. The box labeled "Control" measures the combined signal level using an RF detector and maximizes it by adjusting the phase shifter control voltages.

On our system we decided to implement a model-free gradient descent beamforming algorithm which requires as input only the combined RF signal [2, 3]. This provides significant cost savings for an array with many elements, such as 17 in our case, compared with similar algorithms like the well-known least mean squares (LMS) algorithm [6] which requires knowledge of the individual antenna elements signal powers. The control algorithm falls in the class of gradient-free stochastic approximation (SA) algorithms, more specifically stochastic gradient descent, a general purpose loss function minimization algorithm which has been applied in many fields [7]. Using a model-free algorithm takes care of the many complex, nonlinear and age-dependent system characteristics, such as the phase shifters transfer functions, making costly system calibration and characterization unnecessary.

The control algorithms used in our previous low profile system are implemented digitally and interface with the analog antenna weights and RF power detector using analog/digital converters. In contrast, in the present work we present a gradient descent algorithm which operates and interfaces with the RF components directly in analog domain. We anticipate significant savings in terms of system cost, power consumption, and system integration complexity by switching to an integrated analog implementation, especially for arrays with many elements. For example, in our particular system we would save 34 digital-to-analog converters (DACs) and associated multiplexing hardware, resulting in cost and power savings. In the current system the time spent communicating with the DAC array is a major bottleneck affecting the speed of the algorithm and currently requiring the use of expensive high-speed digital electronics and digital signal processing (DSP). Due to their zero interface overhead and parallel nature, low-cost analog circuits could achieve the same level of performance. Currently, most of the processing performed by the main DSP consists of the beamforming algorithm; offloading this task would permit the use of a lower cost DSP.

Others have also implemented gradient descent algorithms which control an analog or aerial single-output beamformer, but like our previous system, the algorithm is implemented in the digital domain [8–10]. Our work is most similar to these, with the biggest difference being that we implement the complete algorithm as well as the beamforming operation in analog domain. Neural network analog circuits have been used to perform beamforming [11, 12], but these methods are not applicable to our lower cost single receiver architecture primarily because they require multiple received signals and perform beamforming in baseband. In other application domains, there have been reports of analog very large scale integration (VLSI) implementations

[1] The distinction between analog and digital control is highlighted in Fig. 1. In our beamforming approach the analog output of the RF detector is used to control the weights of the phase shifters, while in digital control [4, 5] this signal is sampled and converted to a digital signal that then is used to control the analog phase shifters.

[2] Note that each subarray is connected to one analog phase shifter, and hence each subarray is considered as an antenna in the beamforming procedure.

of gradient descent algorithms. For example [13–17] present gradient descent analog signal processors for training analog VLSI neural networks, and [18] presents a method of tuning analog filters using a similar analog processor. Our work brings techniques from these domains to achieve a novel fully analog solution for performing blind, zero-knowledge, adaptive beamforming. We envision a beamforming radio frequency integrated circuit (RFIC) containing a gradient descent algorithm alongside a large array of analog phase shifters and LNAs which would replace a significant portion of the beamforming hardware and software in various antenna array systems.

This paper presents simulation and experimental results using a four-element antenna array. Only four of the 17 elements were used as a preliminary proof of the concept. Experiments and simulations were conducted in the elevation plane only. Section II contains background information about our low profile phased array system. Section III describes the theory of the analog algorithm followed by simulation results in Section IV. Section V describes the physical implementation followed by experimental results in Section VI. Finally, Section VII concludes the paper.

II. ULTRA LOW PROFILE PHASED ARRAY SYSTEM FOR MOBILE SATELLITE RECEPTION

We have recently developed a 6 cm tall, low-cost phased array for Ku-band satellite TV reception on moving vehicles which uses mechanical tracking and a unique blind, zero-knowledge electronic beamforming algorithm [2, 3]. A photograph of the system is shown in Fig. 2, and the specifications are summarized in Table I. The elevation range makes the array suitable for reception anywhere in North America. Experiments have shown that medium-sized cars may turn as fast as $60^\circ/s$ with an angular acceleration of up to $100^\circ/s^2$. The current hybrid system can compensate for disturbances of up to $60^\circ/s$ with an angular acceleration of up to $85^\circ/s^2$.

The system performs tracking in both the azimuth and elevation planes. In the elevation plane the receiver's latitude is obtained via a GPS unit, and a fixed elevation motor adjustment is performed. Further tracking in the elevation plane is performed only by electronic beamforming, which is sufficient because of the large beamwidth and scan range in this plane. In the azimuth plane a gyro and a stepper motor are used to form a closed-loop mechanical control system which works in tandem with the beamforming algorithm. The beamforming algorithm obtains the total combined received signal power using an RF detector and maximizes this measure by performing gradient descent. Since the only input to the algorithm is the total combined signal power, it inherently performs beamforming in both azimuth and elevation planes.

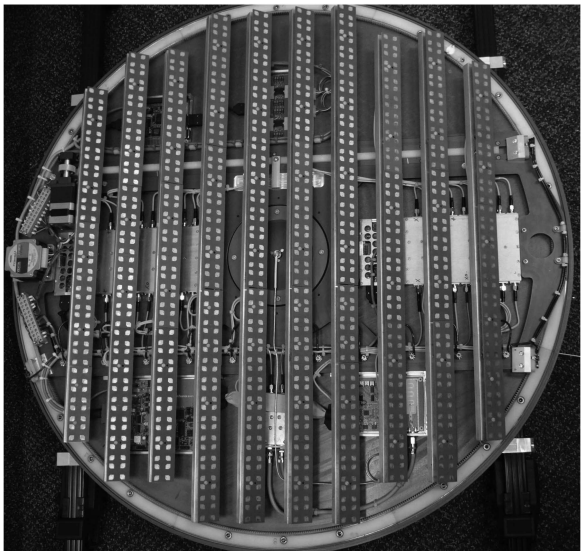

Fig. 2. Low profile antenna system photograph.

TABLE I
Low Profile System Parameters

Parameter	Value
Frequency	12.2–12.7 GHz
Polarization	Dual Circular
Gain	31.5 dB (per polarization)
Axial ratio	< 1.8 dB
Tracking speed (Azimuth)	$60^\circ/s$
Spatial coverage	0°–360° Azimuth 20°–70° Elevation
System height	6 cm
System diameter	86 cm
System weight	12 Kg

One practical issue with using a zero-knowledge algorithm is that the gradient descent operation zeros in on the closest local minimum of the loss function which may not necessarily be the best global configuration. This is solved by higher level control functionality which can reset the algorithm to another initial state if the signal level is considered too low. Once a good signal is initially found, the algorithm is reliable in keeping lock. Since the algorithm performs blind beamforming, it simply maximizes any signal it receives and therefore might track the wrong satellite. To solve this problem, a digital video broadcast (DVB) receiver has been added to the system, permitting the received digital stream to be decoded and the satellite identifier to be extracted. If a lock is obtained on the wrong satellite, action can be taken to control both the mechanical and beamforming algorithms to search for the correct satellite, which takes at most 5 s.

III. ALGORITHM DESCRIPTION

We chose to implement a circuit similar to that described in [17] because it can be easily and directly translated into a simple discrete component circuit

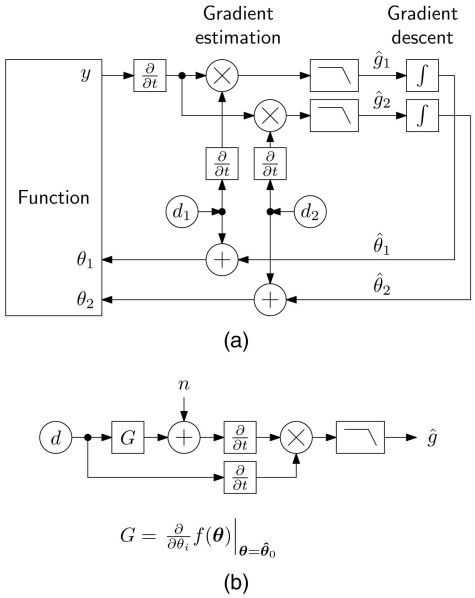

Fig. 3. Continuous-time gradient descent by simultaneous perturbation. (a) Continuous-time gradient descent optimization. (b) Open-loop single weight gradient estimation.

suitable for prototyping. Fig. 3(a) shows the block diagram of the continuous-time algorithm. Only two weights are shown for clarity. $\mathbf{d}$ is a p-dimensional column vector of mutually-orthogonal, zero-mean, small-amplitude dither signals (the perturbation). Reference [13] provides an analysis of the optimality of these signals and compares several practical realizations. Reference [19] mentions the possibility of using sinusoidal signals of different frequencies. In [17] and in this work, these signals are zero-mean, uncorrelated random signals produced as in [20]. The gradient descent operation is straightforward: the discrete-time summation is converted to integration.

Reference [17] provides an analysis of the multidimensional gradient estimation operation. Here we adopt a description consisting of multiple parallel scalar gradient estimation operations resembling the distributed formulation of [13]. If one disconnects the gradient descent part of the circuit and fixes $\hat{\boldsymbol{\theta}}$ at a constant operating point $\hat{\boldsymbol{\theta}}_0$, the gradient estimation operation may be considered an open-loop operation, and the function is reduced to the linear function $f(\mathbf{d}) = \mathbf{g}(\hat{\boldsymbol{\theta}}_0)^T\mathbf{d} + \mathbf{C}$. Ignoring the dc term and noting that the gradient is a constant vector, we may write the function as follows: $f(\mathbf{d}) = \mathbf{G}^T\mathbf{d}$. This shows the combined effect of the individual dither sources on the function output.

If we look at the ith branch, given the fact that all dither components are statistically independent, we can combine the effect of all the other $p-1$ dither noise sources $\mathbf{d}_j$, $j \neq i$ into a single scalar noise n_i. (To this we can also add any other random effect inherent in the measurement of the loss function.) Now the p-dimensional system can be separated into p parallel scalar systems. The gradient estimation part is shown in 3(b). Below we show that output g is a nonbiased estimate of the $G = \mathbf{G}_i$. Since all problems are identical, subscript i is dropped from the following derivation

$$\begin{aligned}\frac{\partial(dG+n)}{\partial t}\frac{\partial d}{\partial t} &= \frac{\partial(dG+n)}{\partial d}\left(\frac{\partial d}{\partial t}\right)^2 \\ &= \left(G+\frac{\partial n}{\partial d}\right)\left(\frac{\partial d}{\partial t}\right)^2 \\ &= G\left(\frac{\partial d}{\partial t}\right)^2 + \frac{\partial n}{\partial d}\left(\frac{\partial d}{\partial t}\right)^2 \\ &= G\left(\frac{\partial d}{\partial t}\right)^2 + \frac{\partial n}{\partial t}\frac{\partial d}{\partial t}. \end{aligned} \tag{1}$$

Taking the expectation of this expression,

$$\begin{aligned}E\left\{\frac{\partial(dG+n)}{\partial t}\frac{\partial d}{\partial t}\right\} &= GE\left\{\left(\frac{\partial d}{\partial t}\right)^2\right\} \\ &\quad + E\left\{\frac{\partial n}{\partial t}\right\}E\left\{\frac{\partial d}{\partial t}\right\} \\ &= GE\left\{\left(\frac{\partial d}{\partial t}\right)^2\right\}. \end{aligned} \tag{2}$$

In Fig. 3(b) a low-pass filter is used to perform a time-limited averaging, a short term expectation operation. The output of the system in Fig. 3(b) is G scaled by the variance of the dither source. p parallel copies of this system will compute an estimate of the p-dimensional gradient $\mathbf{G} = \mathbf{g}(\hat{\boldsymbol{\theta}}_0)$ of the loss function at the point $\hat{\boldsymbol{\theta}} = \hat{\boldsymbol{\theta}}_0$. Closing the loops with p integrators results in p identical scalar optimizers working in parallel, each trying to adjust its own weight.

IV. SIMULATION

The problem was decomposed into two halves: the target function which needs to be optimized and the optimizer. This separation was reflected in the construction of the final system: the four variable optimizer board (a single PCB) connects to the antenna function and maximizes the received signal power. The antenna array existed before this work began and, beyond a simple model used for simulation, is outside the scope of the present work. The focus is on the optimizer.

A. Optimizer

The optimizer (Fig. 3) was modeled as closely as possible to the actual implementation. The implementation consisted of discrete analog components. The basic building block used was the

op-amp. Models were built for the time derivative, time integration, and low-pass filter using basic ideal op-amp circuits which can be found in any circuit textbook. All passive components and accurate op-amp data-sheet characteristics were used for the model. An ideal multiplier was used in the simulation.

B. Antenna Function

The real-world function (which is the motivation of this work) called the antenna function is any function from the family of functions that provides a received RF signal power measurement from the output of the antenna array as a function of the phase shifter voltages (refer to Fig. 1). Many elements which make up this function are fixed, e.g., the antenna elements and their antenna pattern, the LNA characteristics, and the antenna array geometry, but others are not, e.g., the array orientation with respect to the transmitter, the atmospheric conditions, and the satellite transmitted power. We can group all variables which are not the function inputs but which have an effect on the function output and call them function parameters. Furthermore, we can assume the function parameters are constant during the short duration of time it takes to solve for the function maximum. In other words, we can work with the assumption that the received signal strength is only a function of the phase voltages. However, it remains important to see how the optimizer tracks a changing function, for example as the antenna orientation changes with respect to the satellite direction.

A very simple antenna function model was constructed. The first block is composed of one pair of series ideal phase shifters and models everything up to the voltage signals at the outputs of the LNAs; this includes the electromagnetic environment, antenna orientation, array geometrical configuration, phase shifter phase errors, phase shifts due to mismatched path lengths, etc. The resulting four voltages, indexed by i, are $v_i = e^{j\pi(x_i - x_{io})}$, where x_i are the function inputs and x_{io} are the function parameters. We place no restriction on x_{io} even though in reality, given various constraints, only a limited subset of these functions could exist. The power combiner is modeled as a 5-port power combiner built using three ideal 3-port Wilkinson power dividers [21]. After the power combining, an LNB is used to step the frequency down and add further gain. The gain will add a dc offset after logarithmic power detection, so for simplicity a unity gain is assumed, or in other words, the LNB is ignored. Then a single RF detector (the AD8317 logarithmic detector from Analog Devices) is used to measure the total received power. Starting with the data sheet of the RF detector, applying minor signal conditioning on the output, ignoring any dc offset at the output, and the result will typically be $0.88\log(P_{\text{in}})$ V which is the final output y of the function. Substituting all the individual components and normalizing to obtain a maximum value of zero, we obtain the following model for the antenna function $y = f(x_1, x_2, x_3, x_4)$:

$$y = 0.88\log\left(\frac{1}{16}\left|\sum e^{j\pi(x_i - x_{io})}\right|^2\right) \text{ V}. \tag{3}$$

C. Analog Noise Sources

For this application we used an efficient and simple method of generating the dither noise signals, which is described by [20]. Using only a single 25-bit linear feedback shift register (LFSR), 32 mutually-uncorrelated digital bit sequences may be generated by carefully selecting the LFSR seed and XOR-combined taps. Each digital bit sequence is passed through a passive RC filter to produce a zero-mean analog noise signal. Since the random bit sequence has a flat spectrum, the spectrum of the output analog noise signals resembles the transfer function of the filter. All 32 noise sources generate the same master bit sequence, but the bit sequences are delayed such that they are mutually uncorrelated for a period of time much longer than the expected convergence time of the algorithm, approximately $2^{25}/32$ bits. The master bit sequence repeats after 2^{25} bits, a period during which the autocorrelation is almost zero.

D. Simulation Results

All the aforementioned system blocks were modeled using an Agilent ADS circuit simulator. To estimate the behavior of the smart antenna system, a transient simulation is performed using a step change between two antenna functions. Recall the antenna function (3) parametrized by x_{io}. One weight is kept constant at $x_4 = x_{40} = 0$, forming a three variable function. Two functions $f_1(.)$ and $f_2(.)$ are created by choosing two sets of parameters $\{x_{i0}\}_1$ and $\{x_{i0}\}_2$. At time zero an instantaneous step occurs from $f_1(.)$ to $f_2(.)$, starting from an initial state where the algorithm is fully converged on the maximum of $f_1(.)$. The results show how the algorithm converges on the maximum of $f_2(.)$. The 90% convergence time occurs a little bit beyond the recorded simulation time and is estimated at about 30 ms. The simulation result appears in Fig. 4.

V. IMPLEMENTATION

Fig. 5 shows a photograph of the four-subarray smart antenna system used in our experiments. The subarray consists of 2×16 microstrip square patches with two truncated corners. The microstrip antenna subarray is used due to its ease of manufacturing, low cost, low profile, and light weight. The circular

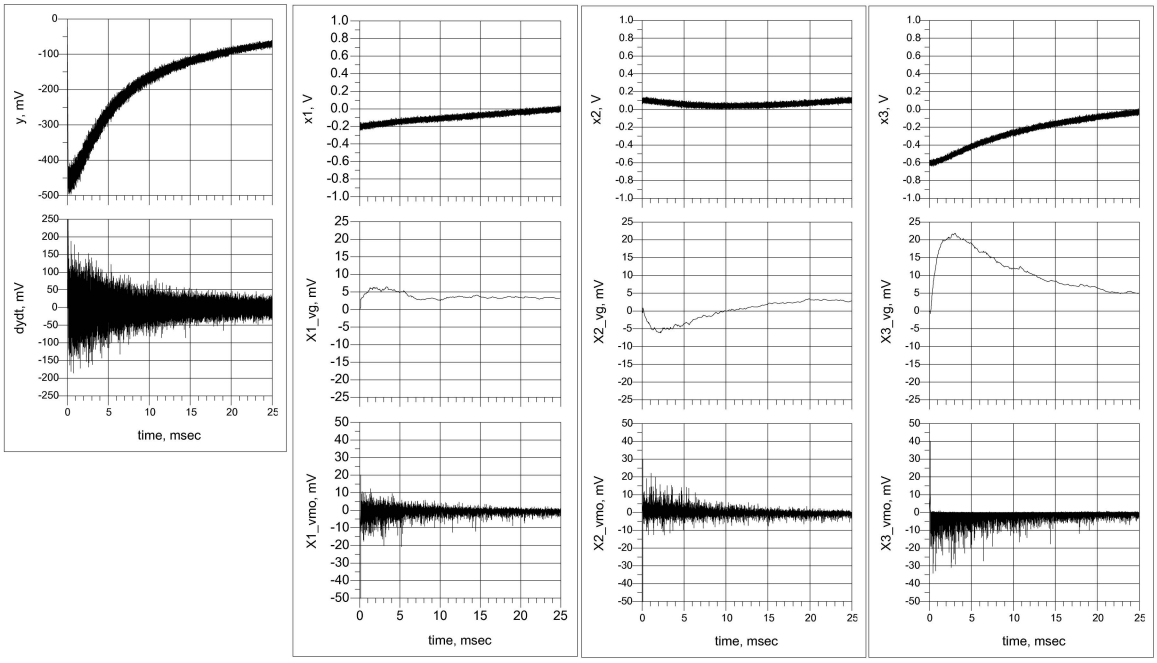

Fig. 4. Simulation of antenna function transient response. Left column displays function output and its time derivative. Remaining three columns describe three function variables x_i. For each variable three plots are shown: variable value (top), instantaneous gradient estimate measured at output of multiplier (bottom), and averaged gradient estimate produced after low-pass filter (middle). Instantaneous gradient (bottom plot) is shown inverted.

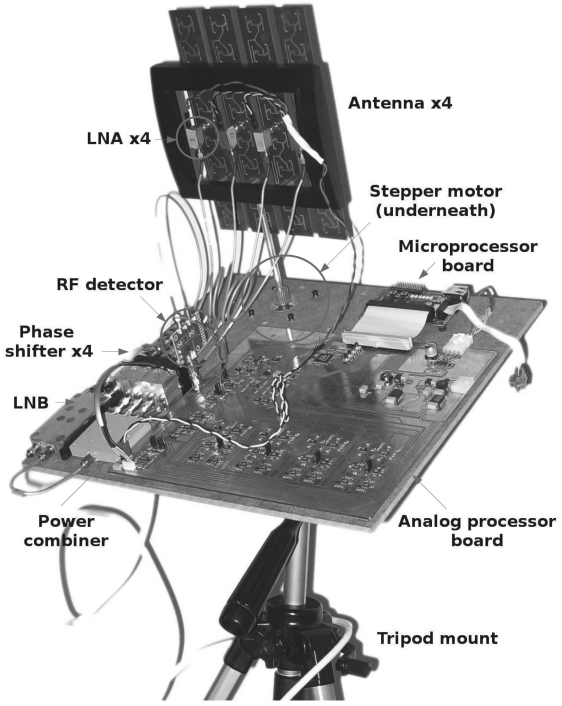

Fig. 5. Smart antenna system experimental setup.

polarization is achieved by employing the sequential rotation technique [22] in which each patch is excited at a single feed point. The elements of the subarray are fed by a corporate microstrip feed network in order to keep the overall constructional complexity at a minimum and maintain a compact size.

The radiation characteristics of these subarrays are measured using the near-field technique. Figs. 6(b)–(d) illustrate the results of these measurements in the principal planes of the subarray at 12.7 GHz. The measured circular polarization gain of the 2×16 subarray is about 19.7 dBi. The loss added by the surface mount connector is estimated to be 0.5 dB at this frequency. Therefore, the actual gain is 20.2 dBi. The half power beamwidth (HPBW) in the $\phi = 90°$ plane according to Fig. 6(c) is approximately $\pm 2.8°$. The HPBW in the $\theta = 90°$ plane is $\pm 20°$.

Fig. 7 shows a block diagram of the optimizer board. Only two variables are shown for clarity. The dashed box outlines a one-variable optimizer, the main unit of which is duplicated p times to produce a p-variable optimizer; for this implementation $p = 4$. The board has a stepper motor interface, a digital interface, as well as an analog function interface. The digital interface consists of a parallel interface and a serial peripheral interface (SPI). The parallel interface connects to a complex programmable logic device (CPLD), which provides control of the test function, analog switches, stepper motor, and many other simple on-off type functions on the board. The SPI interface provides direct access to the DACs and analog-to-digital converters (ADCs). The CPLD also generates the digital pseudorandom noise sources which, after being filtered, become the analog dither noise sources.

The block labeled "test function" implements a two-dimensional test function used for verifying the

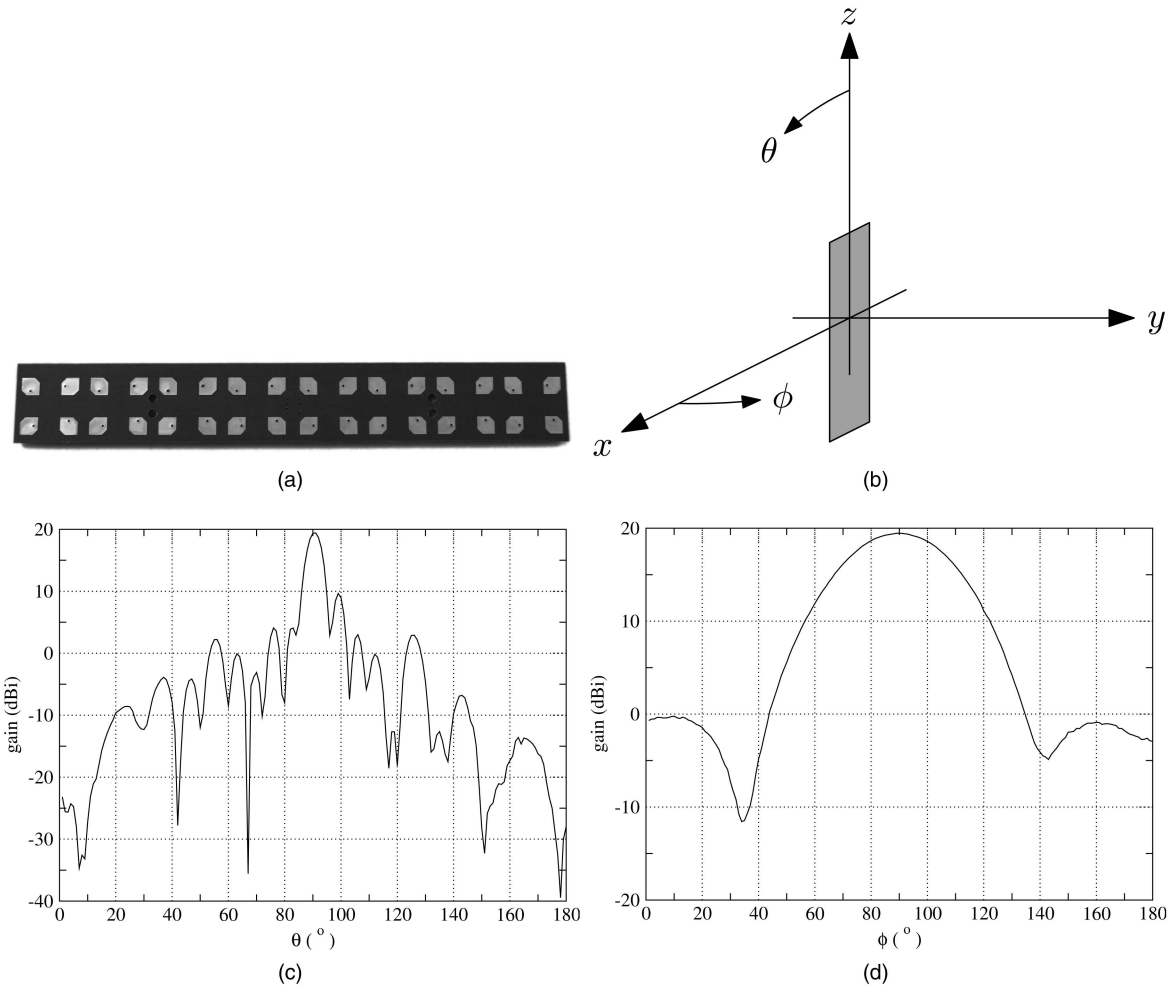

Fig. 6. Antenna subarray layout and radiation pattern. (a) Subarray photograph. (b) Radiation pattern coordinate system. (c) Radiation pattern in $\phi = 90°$ plane. (d) Radiation pattern in $\theta = 90°$ plane.

algorithm using a very simple and precisely known quadratic function. One switch selects between the test function and antenna function as the target function. The function output can be sampled using an ADC and the data transferred to a computer.

The block diagram shows two one-variable optimizer units, one outlined by a box. A high-pass filter is applied to the noise implementing the time-derivative operation. The result is multiplied by the identically filtered output of the target function. The next step is low-pass filtering which completes the gradient estimation. The gradient estimate is passed through an integrator to produce the gradient descent operation by which the function variables migrate to their optimum values. The loop can be broken with the switch, and the function variable can be controlled by software using a DAC, an essential functionality for performing various tests and trying software-based algorithms. The variable can be sampled using an ADC and the data transferred to a computer. The last operation is a variable scaling and shifting to meet the requirements of the external target function, in this case, the phase-voltage characteristics of the phase shifter.

A micro-processor board connects to the digital interface providing higher level time-critical functionality to the system such as data collection from the ADCs. A computer connects to the micro-processor board using a serial port. The software on the computer accesses the low-level simple functional building blocks provided by the CPLD and the micro-processor.

VI. EXPERIMENTAL RESULTS

The smart antenna system was tested outside using a satellite signal. The response to different initial states, as well as the response to changing target functions were measured. The analog algorithm was compared with a similar digital algorithm implemented in software on the computer. The software algorithm is the finite difference stochastic approximation (FDSA) described in [7]. The SPSA has several application-dependent parameters which affect convergence speed and accuracy. Our goal was to compare the digital and analog algorithms in terms of accuracy. Therefore the parameters were chosen

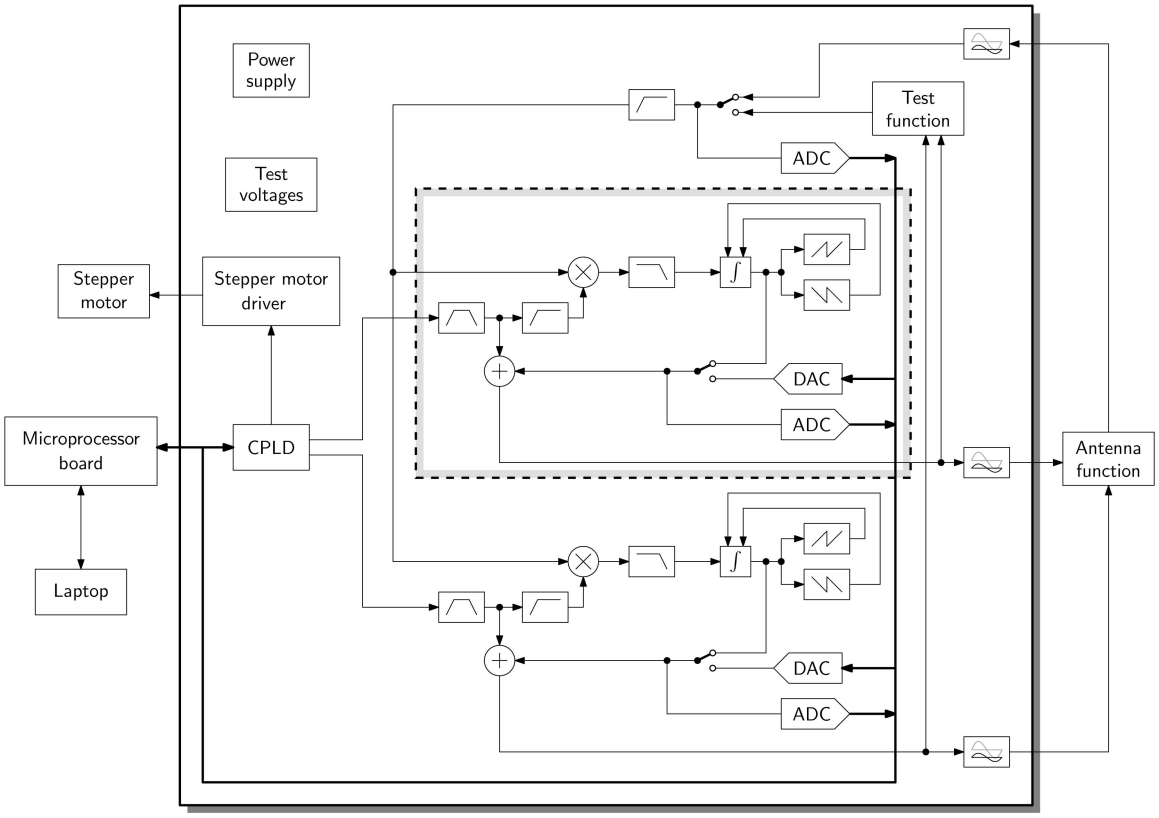

Fig. 7. Optimizer board block diagram.

to make the gradient estimation very accurate at the expense of speed. Typical convergence time is about 30 s.

Keeping with the convention established thus far, all results will show the function variables and output voltages. All signals have a valid range of $(-1,1)$ V. One should keep in mind that in the case of the antenna function, the phase angle is approximately equal to πx_i and the function output y is related to the received signal power by the approximate relation $y = 0.88\log(P_{\text{in}})$ V or equivalently 88 mV per dB. These approximate relationships are based on typical measurements, but were not accurately characterized or calibrated, an important future task. Precise knowledge of the actual received signal power is not important to the convergence speed or accuracy. Being a logarithmic detector, an error in absolute value represents the addition of a constant term to the cost function, which is irrelevant to the optimization problem. An error in the sensitivity would affect the gradient estimate and hence the convergence speed, but this is easily compensated for by a closed-loop gain adjustment.

A. Received Signal Strength versus Pointing Direction

The goal is to measure the signal strength received by the smart antenna as a function of the mechanical pointing deviation from the ideal. One mechanical axis is fixed, while the second axis permits the antenna orientation to be scanned between -5.4° through 5.4° with respect to the perpendicular orientation towards the satellite. The position scanning is performed from the left angle (negative) through the perpendicular (zero) to the right angle (positive).

An important reference point is the maximum achievable signal level. Given that the antenna elements have maximum gain in the direction perpendicular to the antenna plane, the maximum achievable signal level from the smart antenna should occur when the satellite direction is perpendicularly incident on the antenna array plane, while the phases are such that the individual signals combine in phase. This was achieved by the following calibration procedure. Starting with all phases fixed at zero, the antenna array is pointed optimally towards the satellite. The digital algorithm is then performed, and the solution is frozen. Again the antenna array is pointed optimally. This is repeated until there is no more observed improvement in signal strength. The resulting mechanical orientation of the antenna is called the perpendicular position, and the resulting phase shifter phases is called the perpendicular phases.

The first experiment establishes a reference point. The received signal strength is measured as a function of orientation when the algorithm is off. The phases are fixed at the perpendicular phases,

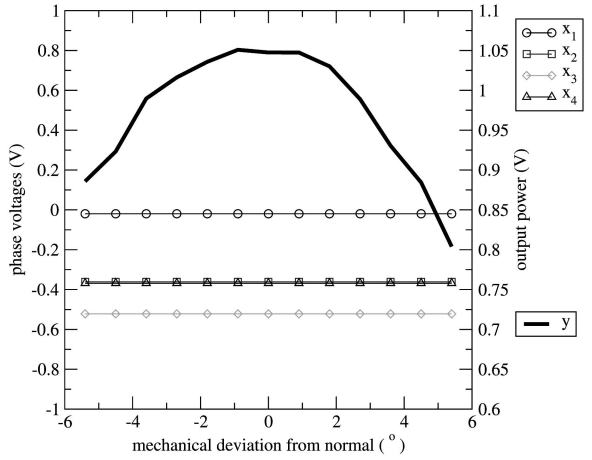

Fig. 8. Received signal power versus antenna pointing direction using fixed phases.

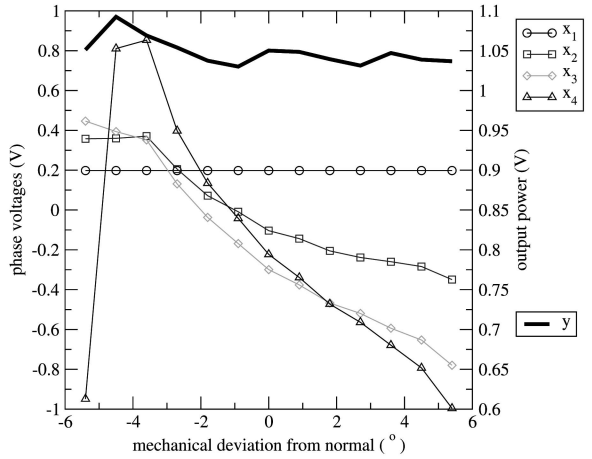

Fig. 9. Received signal power versus antenna pointing direction using analog optimizer.

and the antenna array is moved to the left and right of the perpendicular position. The result is shown in Fig. 8. As expected the signal is strongest at the perpendicular position and drops off on either side. This figure is to be used as a reference for comparing the improvements obtained with various adaptive algorithms.

In the next experiment the analog optimizer is turned on for all phases except the phase corresponding to x_1. The analog optimizer is initialized only once at the beginning of the experiment (at the perpendicular orientation) after which it is kept operating for the remainder of the experiment. The results are presented in Fig. 9. The received power level never drops below 1.025 V, a big improvement over the result obtained with the fixed phases (Fig. 8). The phase corresponding to x_4 experiences positive wrap-around, a functionality implemented on the optimizer board to ensure that the function variables stay within the $(-1,1)$ V domain.

In the next experiment the digital optimizer is turned on for all phases except the phase

TABLE II
Comparison of Received Signal Strength Over Scanned Antenna Angle

	Received Signal Strength (V)		
Algorithm	min	avg	max
Digital	1.03	1.05	1.09
Analog	1.02	1.04	1.06

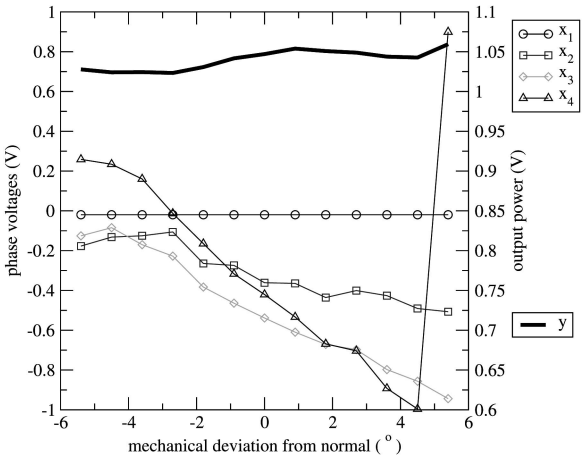

Fig. 10. Received signal power versus antenna pointing direction using digital optimizer.

corresponding to x_1. The digital optimizer is initialized only once at the beginning of the experiment (at the perpendicular orientation). After waiting for the algorithm to converge, the algorithm is stopped and the antenna is positioned at the most negative angle. The algorithm is then allowed to continue until it again converges, after which it is stopped and the resulting power is recorded. This is repeated for every angle. The results are presented in Fig. 10. Comparing Figs. 9 and 10 it is evident that the digital optimizer finds a different solution than the analog optimizer. However, as summarized in Table II, in terms of maximizing the received signal power, the analog optimizer performs virtually identically as well as the digital optimizer.

B. Transient Tests

Transient experiments were performed to capture more detailed information about the optimization process. Here we are interested not only in the final solution after the algorithm has converged, but also in the path taken by the weights during the optimization process, the convergence time, and any other irregularities such as overshoot and glitches.

The first experiment tests the algorithm convergence from random initial states. The antenna is pointed optimally, the phases are initialized with random values, and the algorithm is turned on. After convergence, the algorithm is stopped, the phases

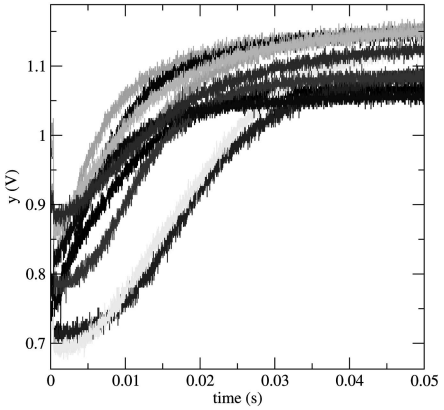

Fig. 11. Antenna function transient response from random initial state.

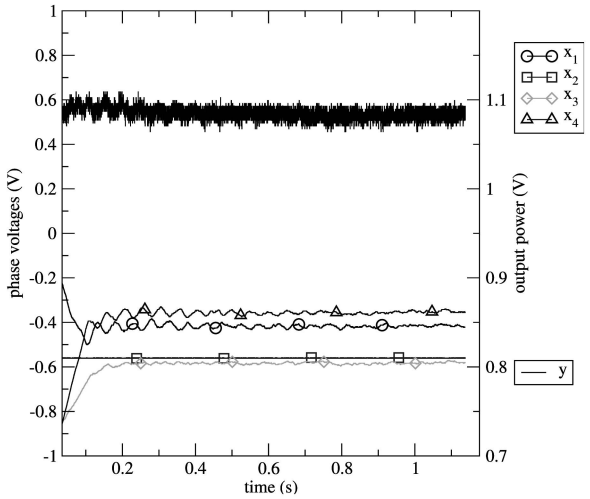

Fig. 12. Antenna function transient response to motor 6.3° step.

are reinitialized with new random values, and the process is repeated. Fig. 11 shows the received signal power in several recorded outcomes. It is apparent that the algorithm convergence time depends on the initial state. Furthermore, the final convergence value also depends on the initial state. In all outcomes convergence occurs in less than approximately 50 ms. Because of the varying results depending on the initial state, only a rough comparison with the simulation is possible. The simulation result from Fig. 4 fits with some of the outcomes of Fig. 11.

What seems to be indisputable is the fact that the analog function has multiple local maxima which were not modeled by the simple analog function described by (3). One possible explanation may be that the antenna array sometimes creates a beam towards neighboring satellites depending on its initial state. This possibility should be modeled and investigated further. Another explanation, which does not exclude the previous one, could be found in the phase-shifter phase-gain relationship. Whereas the phase shifter was modeled as $y = e^{j\pi x}$, the actual model looks like $y = f(x)e^{jg(x)}$. Function $g(x)$ is a monotonically increasing function, and besides an effect on the convergence rate, the final value should not be affected. On the other hand, function $f(x)$ can cause multiple solutions since a nonaligned phase may be preferred over the aligned phase due to much greater gain. An improved phase shifter model should definitely be included in future simulations.

The next experiment tests the algorithm convergence with a changing antenna function. One practical method of changing the antenna function is to reorient the antenna using the stepper motor. The experiment description is as follows: orient the antenna optimally, turn on the algorithm, and achieve convergence; then apply a rapid 6.3° mechanical deviation from normal using the stepper motor and watch the algorithm convergence. The results, including all phases and function output, are shown in Fig. 12. For this test we would have preferred a true step input, but the mechanical dynamics do not permit this, resulting in a 6.3° step having a duration of approximately 100 ms. The algorithm manages to maintain an almost constant received signal power by adjusting the phases very rapidly (< 200 ms). The observed ringing is due to the mechanical vibrations caused by the intensity of the step, a phenomenon which is visible. The result of this experiment shows that the smart antenna can adapt its pattern to compensate for changes in orientation at rates in excess of $60°/s$.

VII. CONCLUSIONS

We have presented a low-cost, low power consumption, and sufficiently fast analog adaptive controller which performs gradient descent using a simple continuous-time analog circuit. To verify the performance of the proposed controller, it has successfully been implemented and tested in a Ku-band satellite TV antenna array. This brings analog gradient descent optimization into the field of antenna beamforming, resulting in reduced system cost and power consumption and simpler VLSI integration. The algorithm has no knowledge of the target function and can therefore be used in various other beamforming applications.

Simulations showed convergence times in the order of 30 ms. The system was tested outdoors in a realistic scenario with a satellite signal. Experimental results showed convergence times between 30 and 50 ms, resembling the simulations. The analog algorithm adapts the antenna pattern to achieve fast tracking speeds $> 60°/s$. In terms of convergence accuracy, the results were very similar to those obtained using a software implementation of a stochastic approximation algorithm.

Future efforts will be devoted to improved global convergence, circuit optimization for even faster

performance, and a specialized VLSI implementation for smart antenna applications consisting of the analog algorithm as well as RF components.

MIRCEA HOSSU
3563 Autumnleaf Cres.,
Mississauga, Ontario, Canada
L5L1K6
E-mail: (mirea@maxwell.uwaterloo.ca)

S. HAMIDREZA JAMALI
PEDRAM MOUSAVI
KIARASH NARIMANI
MOHAMMAD FAKHARZADEH
Intelwaves Technologies Ltd.
470 Weber Street North
Waterloo, Ontario, Canada

SAFIEDDIN SAFAVI-NAEINI
University of Waterloo
Waterloo, Ontario, Canada

REFERENCES

[1] Hossu, M., Jamali, S. H., Mousavi, P., Narimani, K., Fakharzadeh, M., and Safavi-Naeini, S.
Microwave beamforming using analog signal processing.
In *Proceedings of the IEEE Antennas and Propagation Society International Symposium 2008*, July 2008, 1–4.

[2] Fakharzadeh, M., Safavi-Naeini, S., Jamali, S. H., and Mousavi, P.
Zero-knowledge beamforming of phased array antennas based on simultaneous perturbation gradient approximation.
In *Proceedings of the IEEE Antennas and Propagation Society International Symposium 2006*, July 2006, 537–540.

[3] Mousavi, P., Fakharzadeh, M., Jamali, S. H., Narimani, K., Hossu, M., Bolandhemmat, H., Rafi, G., and Safavi-Naeini, S.
A low-cost ultra low profile phased array system for mobile satellite reception using zero-knowledge beamforming algorithm.
IEEE Transactions on Antennas and Propagation, **56** (Dec. 2008), 3667–3679.

[4] Ohira, T.
Analog smart antennas: An overview.
In *Proceedings of the 13th IEEE International Symposium on Personal, Indoor and Mobile Radio Communications*, vol. 4, Sept. 2002, 1502–1506.

[5] Ohira, T. and Cheng, J.
Analog smart antennas.
In S. Chandran (Ed.), *Adaptive Antenna Arrays: Trends and Applications*.
New York: Springer, 2004, 184–204.

[6] Widrow, B., Mantey, P. E., Griffiths, L. J., and Goode, B. B.
Adaptiye antenna systems.
Proceedings of the IEEE, **55**, 12 (1967), 2143–2159.

[7] Spall, J. C.
Introduction to Stochastic Search and Optimization.
Hoboken, NJ: Wiley, 2003.

[8] Cheng, J., Kamiya, Y., and Ohira, T.
Adaptive beamforming of ESPAR antenna using sequential perturbation.
2001 IEEE MTT-S International Microwave Symposium Digest, **1** (2001), 133–136.

[9] Sun, C., Hirata, A., Ohira, T., and Karmakar, N. C.
Fast beamforming of electronically steerable parasitic array radiator antennas: Theory and experiment.
IEEE Transactions on Antennas and Propagation, **52** (July 2004), 1819–1832.

[10] Wennstrom, M., Strandell, J., Oberg, T., Lindskog, E., and Rydberg, A.
Auto-calibrating adaptive array for mobile telecommunications.
IEEE Transactions on Aerospace and Electronic Systems, **36** (Apr. 2000), 729–736.

[11] Chang, P-R., Yang, W-H., and Chan, K-K.
A neural network approach to MVDR beamforming problem.
IEEE Transactions on Antennas and Propagation, **40** (Mar. 1992), 313–322.

[12] Du, K-L., Lai, A. K. Y., Cheng, K. K. M., and Swamy, M. N. S.
Neural methods for antenna array signal processing: A review.
Signal Processing, **82**, 4 (2002), 547–561.

[13] Dembo, A. and Kailath, T.
Model-free distributed learning.
IEEE Transactions on Neural Networks, **1** (Mar. 1990), 58–70.

[14] Cauwenberghs, G.
A fast stochastic error-descent algorithm for supervised learning and optimization.
In *Proceedings of the Conference on Advances in Neural Information Processing Systems 5*, San Francisco, CA, 1993, 244–251.

[15] Cauwenberghs, G.
An analog VLSI recurrent neural network learning a continuous-time trajectory.
IEEE Transactions on Neural Networks, **7** (Mar. 1996), 346–361.

[16] Alspector, J., Meir, R., Yuhas, B., Jayakumar, A., and Lippe, D.
A parallel gradient descent method for learning in analog VLSI neural networks.
In *Proceedings of the Conference on Advances in Neural Information Processing Systems 5*, San Francisco, CA, 1993, 836–844.

[17] Kirk, D. B., Kerns, D., Fleischer, K., and Barr, A. H.
Analog VLSI implementation of multi-dimensional gradient descent.
Neural Information Processing Systems, **5** (1993), 789–796.

[18] Carusone, A. C. and Johns, D. A.
Analog filter adaptation using a dithered linear search algorithm.
In *Proceedings of the International Symposium on Circuits and Systems* (ISCAS), vol. 4, 2002, 269–272.

[19] Widrow, B. and McCool, J.
A comparison of adaptive algorithms based on the methods of steepest descent and random search.
IEEE Transactions on Antennas and Propagation, **24**, 5 (1976), 615–637.

[20] Alspector, J., Gannett, J. W., Haber, S., Parker, M. B., and Chu, R.
A VLSI-efficient technique for generating multiple uncorrelated noise sources and its application to stochastic neural networks.
IEEE Transactions on Circuits and Systems, **38** (Jan. 1991), 109–123.

[21] Pozar, D. M.
Microwave Engineering.
Hoboken, NJ: Wiley, 1998.

[22] Huang, J.
A Ka-band circularly polarized high-gain microstrip array antenna.
IEEE Transactions on Antennas and Propagation, **43**, 1 (1995), 113–116.